

Luminescent AlN Semiconductor Nanocrystals

Hannah F. Gaiser, Felix Jung, Radian Popescu, Matthias Steurer, Dagmar Gerthsen, and Claus Feldmann*

Aluminum nitride III-V semiconductor nanoparticles are prepared in the liquid phase via a two-step synthesis. In a first step, a mixed amide-imide intermediate is prepared in liquid ammonia. In a second step, the ammonolysis is completed by microwave heating at 300 °C in [BMIm][NTf₂] as an ionic liquid to obtain crystalline β -AlN, which is usually known as a high-pressure phase. The nanoparticles have a size of 3.7 ± 0.7 nm. Particle size and chemical composition are examined by transmission electron microscopy, energy-

dispersive X-ray spectroscopy, infrared spectroscopy, and X-ray powder diffraction. According to UV-vis spectroscopy and a Tauc plot, a bandgap of 5.2 eV is determined. The AlN nanoparticles show photoluminescence with bluish white emission and a quantum yield of 15%, which is a typical value for core-type semiconductor nanoparticles without a protecting shell. A liquid-phase synthesis of crystalline AlN nanoparticles (<10 nm) showing visible emission at room temperature is reported for the first time.

1. Introduction

With the discovery of blue- and near-UV light-emitting diodes (LEDs),^[1] main-group-metal nitrides such as AlN, GaN, InN, as well as their solid solutions (e.g., (Ga,In)N) have become most relevant for lighting applications. They are used as semiconductors for the direct conversion of electricity into near-UV or blue light.^[2] Besides bulk-type materials, these main-group metal nitrides also came into focus as nanoparticles, which are specifically interesting for thin-film applications.^[3] Besides LEDs and luminescence,^[4] nanosized main-group-metal nitrides are also intensely discussed as semiconductors for photocatalysis and electrocatalysis.^[5]

The synthesis of metal-nitride nanoparticles is challenging with regard to several issues. First of all, conventional syntheses – viz are nitridation (i.e., reaction of metal with nitrogen) and ammonolysis (i.e., reaction of metal oxide with ammonia) – usually require high temperatures (>500 °C) to activate the inert nitrogen or to completely deprotonate ammonia.^[6] Moreover, high crystallinity is needed, which, again, usually requires high temperatures (>500 °C).^[7] High temperatures, however, are counterproductive for preparing nanoparticles since heating also triggers particle growth and agglomeration. High crystallinity and high purity

are also needed to avoid lattice defects and impurities that otherwise lead to undesired energy states in the bandgap, causing non-radiative decay processes.^[8] Finally, the situation is even more difficult for highly oxophilic cations with high charge density, such as Al³⁺, since the high stability of the respective oxides promotes the formation of oxide impurities, for instance, in AlN.

As a result, the realization of crystalline main-group-metal nitride nanoparticles such as AlN at moderate temperatures remains a challenge. Aiming at a liquid-phase synthesis, we here suggest an ionic-liquid-based synthesis of AlN semiconductor nanoparticles. The synthesis was performed at 300 °C under moisture-free conditions in two steps to separate particle nucleation and crystallization. A liquid-phase synthesis of crystalline and luminescent AlN nanoparticles – to the best of our knowledge – is rare until now.


2. Results and Discussion


2.1. Synthesis

Among the III-V-type semiconductors, aluminum nitride/AlN, as a bulk material, has the widest bandgap with 6.2 eV.^[9] Due to the highly oxophilic character of Al³⁺, avoiding oxide impurities (even on a level ≥ 100 ppm) is a specific challenge. Due to the high local Al–N bonding energy and the resulting slow diffusion in the solid state, moreover, the crystallization is an additional challenge. Therefore, AlN nanostructures were most often realized via physical or gas-phase methods (e.g., arc plasma, laser ablation, wire explosion method, vapor-phase epitaxy, and chemical vapor deposition).^[10] These methods typically result in AlN thinfilms. AlN nanoparticles were yet obtained by direct nitridation of aluminum,^[11] ammonolysis of Al₂O₃,^[12] the use of C₃N₄ as a template,^[13] carbothermal reactions, and ammonothermal reactions at high NH₃ pressure (up to 800 bar).^[14] In all cases, the crystallization of AlN required high temperatures (>500 °C) and resulted in highly agglomerated large particles (100 nm up to 5 μ m) with a broad

H. F. Gaiser, F. Jung, M. Steurer, C. Feldmann
Institute for Inorganic Chemistry
Karlsruhe Institute of Technology (KIT)
Engesserstrasse 15, D-76131 Karlsruhe, Germany
E-mail: claus.feldmann@kit.edu

R. Popescu, D. Gerthsen
Laboratory for Electron Microscopy
Karlsruhe Institute of Technology (KIT)
Engesserstrasse 7, D-76131 Karlsruhe, Germany

 Supporting information for this article is available on the WWW under https://doi.org/10.1002/cnma.202500230

 © 2025 The Author(s). ChemNanoMat published by Wiley-VCH GmbH. This is an open access article under the terms of the Creative Commons Attribution License, which permits use, distribution and reproduction in any medium, provided the original work is properly cited.

size distribution. The often applied oxygen-containing starting materials seem disadvantageous anyway since oxide impurities can hardly be avoided. Aiming at a liquid-phase syntheses, AlN nanorods (3×10 nm) were realized in a mixture of trioctylamine and hexadecylamine at 290 °C under high-pressure ammonia only recently.^[15] The resulting AlN nanorods with a certain amount of amorphous material did not show visible emission. Thus, a liquid-phase synthesis of crystalline and luminescent AlN nanoparticles (<10 nm in size) at moderate temperature (≤ 300 °C), to the best of our knowledge, is unknown until now.

Aiming at a liquid-phase synthesis of AlN nanoparticles, first of all, we aimed for strictly avoiding all sources of moisture (e.g., in starting materials, solvents, and atmosphere) (Figure 1). For this purpose, AlCl_3 was selected as the starting material and dissolved in liquid NH_3 at -34 °C together with KNH_2 as a strong base. Due to the acid–base reaction of AlCl_3 and KNH_2 , ammonolysis already occurred at this temperature to result in a mixed amide-imide intermediate $\text{Al}_{n+m}(\text{NH}_2)_n(\text{NH})_m$ in the first step, with – according to elemental analysis – an amide-to-imide ratio around 1:1 (SI: Figure S1, Supporting Information). The colorless suspension was then naturally warmed to room temperature to remove excess NH_3 (Figure 1a).

As a second step, the amide-imide intermediate was dispersed in $[\text{BMIm}][\text{NTf}_2]$ as an ionic liquid (BMIm: 1-butyl-3-methylimidazolium, NTf_2^- : bis(trifluoromethane)sulfonimide) and heated in a microwave oven for 15 min at 300 °C (Figure 1b). The advantage of microwave heating over conventional resistance heating relates to the very fast heating (120 s) and the direct coupling of the microwave radiation into the ionic liquid as a highly polar medium. This fast heating supports a fast conversion of amide-imide intermediate to crystalline AlN nanoparticles, whereas slow heating could cause particle growth and particle agglomeration. Furthermore, the ionic liquid stabilizes the amide-imide intermediate as well as the final AlN nanoparticles against uncontrolled growth and agglomeration.^[16] The high temperature (300 °C) in the aprotic ionic liquid supports the completeness of the ammonolysis and the evaporation of all NH_3 . Here, it needs to be noticed that the observed orange color of the as-prepared suspensions originates from slightly decomposed ionic liquid (Figure 1b). Finally, the colorless AlN nanoparticles were separated by centrifugation and purified by sequential redispersion/centrifugation in/from methanol or acetonitrile (Figure 1c).

2.2. Particle Size and Composition

Particle size, particle shape and size distribution of the as-prepared AlN nanoparticles were determined by transmission electron microscopy (TEM, Figure 2). TEM overview images show uniform nanoparticles with mean diameters of 3.7 ± 0.7 nm (Figure 2a,b). Moreover, high-resolution (HR)TEM images indicate parallel lattice fringes (Figure 2c) that evidence the single-crystalline character of the as-prepared AlN. According to the observed lattice fringe distance of 2.3 Å, the structure of the nanoparticles is compatible with cubic β -AlN (bulk β -AlN with $d_{1-10} = 2.27$ Å).^[17] The crystal structure of the β -AlN nanoparticles is also confirmed by 2D-Fourier-transform (2D-FT) analysis (Figure 2d), which is in accordance with the calculated diffraction pattern of cubic rocksalt-type bulk β -AlN in the [101] zone axis (Fm-3m with $a = 3.938$ Å).^[17] Here, it needs to be noticed that β -AlN is a

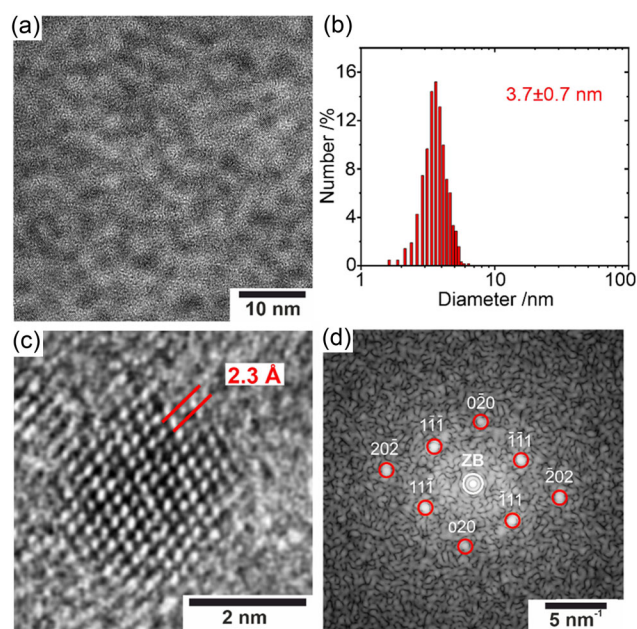


Figure 2. Particle size, particle shape, and particle size distribution of the as-prepared β -AlN nanoparticles: a) Overview TEM image; b) size distribution based on statistical evaluation of >600 nanoparticles on TEM images; c) detailed HRTEM image of a single-crystalline nanoparticle with lattice fringes; and d) 2D-FT of the single-crystalline nanoparticle in (c) and calculated diffraction pattern with Miller indices for rocksalt-type bulk β -AlN (○) in the [101] zone axis (white circle indicates zero-order beam, ZB).

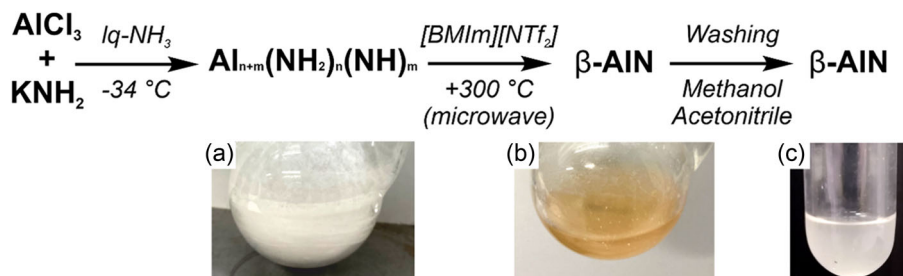


Figure 1. Scheme illustrating the liquid-phase synthesis of β -AlN nanoparticles: a) Reaction of AlCl_3 and KNH_2 in liquid ammonia with precipitation of a colorless mixed amide-imide phase; b) β -AlN suspension in ionic liquid after microwave heating; and c) β -AlN nanoparticle suspension in acetonitrile after washing.

high-pressure phase. Such high-pressure (bulk) phases, however, are often found in the case of nanoparticles, which can be attributed to the internal stress and strain of small-sized particles (<10 nm).^[18] The formation of nanoparticles with the structure of a high-pressure phase was shown before, including carbon nanoparticles crystallizing in the diamond structure type as the most prominent example^[19] or GaN nanoparticles crystallizing in the sphalerite structure type.^[20] The formation of a thermodynamically metastable phase in a liquid-phase synthesis is also in accordance with Ostwald's step rule.^[21] Finally, the absence of reflections beyond those of AlN points to the purity of the as-prepared nanoparticles.

High-angle annular dark-field scanning transmission electron microscopy (HAADF-STEM) images and energy-dispersive X-ray spectroscopy (EDXS) elemental maps of Al (Al- K_{α} line) and N (N- K_{α} line) recorded from an agglomerate of AlN nanoparticles are shown in **Figure 3**. Different intensities in the Al- and N-elemental maps can be correlated with regions of higher intensities in the HAADF-STEM image, which indicate thicker regions in the agglomerate. The quantification of EDXS maps results in 48 ± 3 at-% Al and 52 ± 4 at-% N, which matches well with the expected values of 50 at% Al and 50 at% N for AlN.

Furthermore, the presence and purity of the as-prepared AlN nanoparticles were examined by Fourier-transform infrared (FT-IR) spectroscopy and X-ray powder diffraction (XRD). To this concern, FT-IR spectra generally show low-intensity and broad vibrations (**Figure 4a**). Nevertheless, the strongest

absorption at $600\text{--}400\text{ cm}^{-1}$ coincides with the lattice vibration of crystalline AlN.^[22] Further vibrations at $3700\text{--}3100\text{ cm}^{-1}$ ($\nu(\text{O--H})$), $2970\text{--}2880\text{ cm}^{-1}$ ($\nu(\text{C--H})$), and $1400\text{--}1200\text{ cm}^{-1}$ ($\nu(\text{S=O})$) relate to surface-adhered ionic liquid and methanol from the washing procedure. Methanol is used due to its higher solubility of KCl. XRD only shows background without any specific Bragg reflex (**Figure 4b**). This finding is not a surprise, taking the small particle size (3.7 ± 0.7 nm) and the low scattering power of the AlN nanoparticles into account. To improve the crystallinity and to verify the composition, the as-prepared AlN nanoparticles were annealed in an argon atmosphere at 1200°C . Although not nanosized after this treatment, XRD then clearly shows broad reflections of wurtzite-type α -AlN (SI: **Figure S2**, Supporting Information).^[23] Thus, the metastable β -AlN phase of the as-prepared nanoparticles, observed by HRTEM measurements (**Figure 2c,d**), was thermally converted to the stable wurtzite-type α -AlN, which is in accordance with Ostwald's step rule.^[21] The broad reflections still suggest small crystallite sizes even after annealing.

2.3. Optical Properties

The optical properties of the as-prepared AlN nanoparticles were examined with UV-vis spectroscopy and photoluminescence (PL) spectroscopy. UV-vis spectra indicate a broad absorption below 500 nm (**Figure 5a**), which reflects the light yellow color of powder samples. According to a Tauc plot, a bandgap of 5.2 eV can be

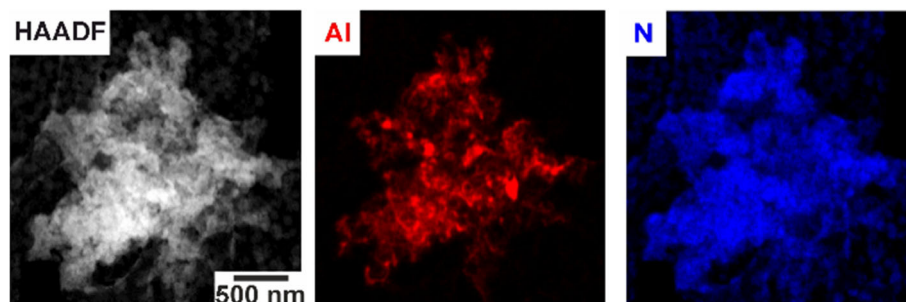


Figure 3. Element distributions of an AlN nanoparticle ensemble: HAADF-STEM image and corresponding EDXS elemental maps of Al (Al- K_{α} line, red) and N (N- K_{α} line, blue).

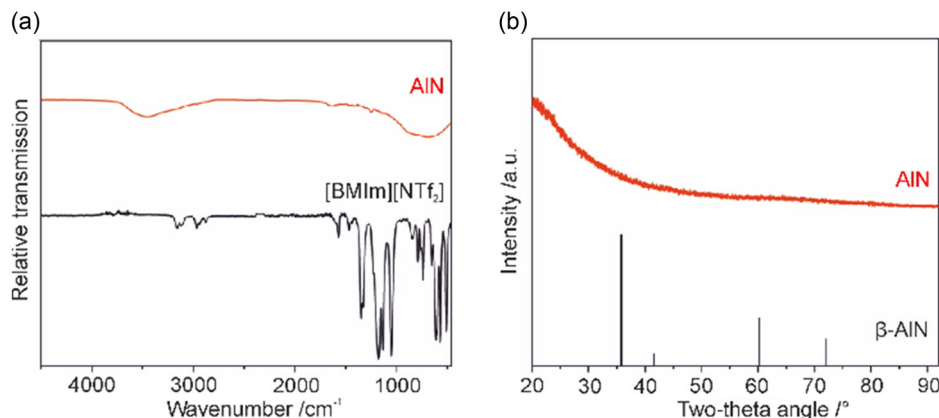


Figure 4. Chemical composition of the AlN nanoparticles: a) FT-IR spectrum ([BMIm][NTf₂] as a reference); and b) XRD (bulk β -AlN as a reference).^[17]

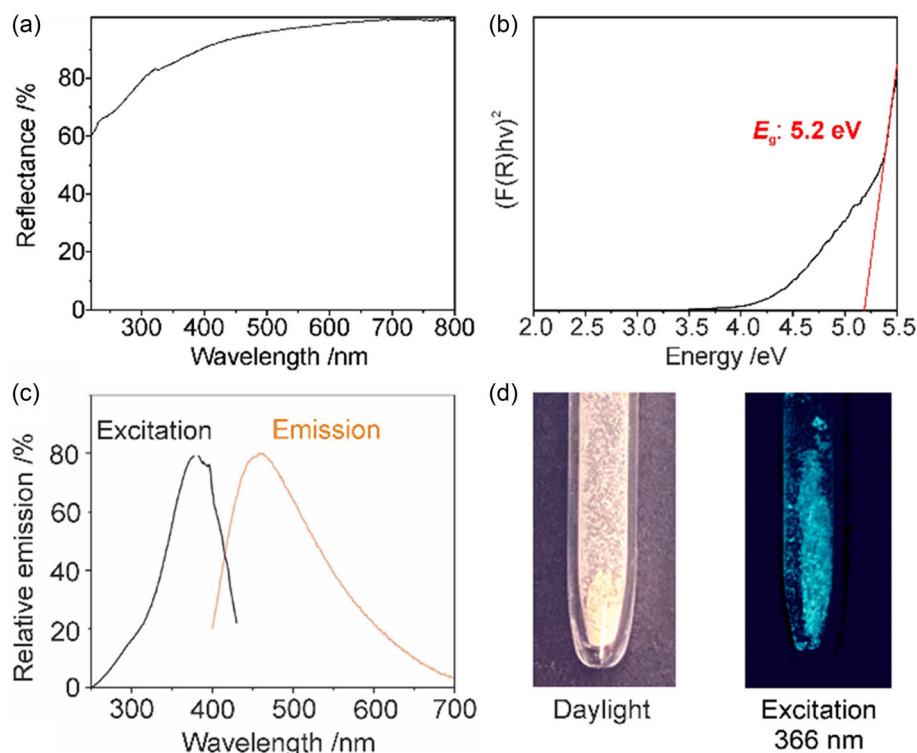


Figure 5. Optical properties of the as-prepared AlN nanoparticles: a) UV-vis spectrum; b) Tauc plot to determine the bandgap; c) PL spectra with excitation (λ_{exc} : 458 nm) and emission (λ_{exc} : 380 nm); and d) photos of powder samples in daylight and under excitation (λ_{exc} : 366 nm).

deduced (Figure 5b), which is below bulk AlN^[9] but well in agreement with nanostructured AlN made via gas-phase techniques (4.0–5.3 eV).^[24] Excitation spectra exhibit strong absorption at 330–450 nm with a shoulder at 250–330 nm (Figure 5c). Here, the shoulder can be attributed to the direct valence-band to conduction-band transition. The corresponding emission spectra indicate broad emission at 400–700 nm with its maximum at 458 nm, which is in accordance with the bluish emission observed under UV excitation (Figure 5d). PL, on the one hand, validates the crystallinity of the as-prepared AlN nanoparticles. The broad absorption and emission band, on the other hand, point to donor-acceptor-type emission and defect states, as they are expected due to the large surface of small-sized nanoparticles. Similar emission at 400 to 600 nm was reported for nanoscale AlN before, with emission maxima at 416, 512, and 599 nm that were similarly attributed to deep-level defects.^[25] These findings are also reflected by a quantum yield of $15 \pm 3\%$, which is the first quantum yield reported for AlN nanoparticles at all. In fact, this is a typical value as it was also observed for II-VI semiconductors such as CdSe in the absence of a core@-shell structure.^[26]

3. Conclusions

The wide-bandgap III-V-semiconductor AlN was prepared via a two-step liquid-phase synthesis. In a first step, AlCl₃ was dissolved in liquid ammonia and reacted with KNH₂ as a strong base to form the mixed amide-imide phase as a colorless intermediate.

After evaporation of NH₃, this intermediate was dispersed in [BMIm][NTf₂] as an ionic liquid and heated in a microwave oven at 300 °C for 15 min. Rapid microwave-driven heating in the ionic liquid, on the one hand, promotes the completion of the ammonolysis and, on the other hand, supports the crystallization of the nitrides. To avoid oxide impurities, all sources of moisture (e.g., starting materials, solvents, and atmosphere) were avoided. According to HRTEM, 2D-FT analysis, and XRD, a high-pressure phase is obtained with β -AlN. Small-sized nanoparticles were obtained with a size of 3.7 ± 0.7 nm.

UV-vis spectroscopy and Tauc plots point to a bandgap of 5.2 eV. The as-prepared crystalline AlN nanoparticles show PL with bluish white emission. The quantum yield of 15% is limited due to surface defects and the large surface area. The observed values are typical for small-sized semiconductor nanoparticles in the absence of a core@shell structure. The realization of crystalline and emissive AlN nanoparticles points to the general potential of the ionic-liquid-based synthesis and points to the option of realizing further nitride-based semiconductor nanoparticles.

4. Experimental Section

Synthesis

General: Synthesis and purification procedures were performed under inert gas (argon), using standard Schlenk techniques or glove boxes. This also includes all centrifugation and washing procedures. Moreover, sample preparation and sample transfer for analytical characterization were strictly performed under inert conditions,

e.g., by using specific transfer modules. Acetonitrile (Carl Roth, $\geq 99.9\%$) was refluxed over CaH_2 onto P_4O_{10} and degassed by three freeze-pump-thaw cycles. KNH_2 was synthesized by reacting potassium (Riedel-de-Haën, 99%) in liquid ammonia (Air Liquide, 99.98%) at -78°C using Fe_2O_3 as a catalyst, followed by filtering and drying under vacuum. Aluminum(III) chloride (Aldrich, 99.99%) was used as purchased. $[\text{BMIm}][\text{NTf}_2]$ was prepared according to literature procedures and dried for several days under reduced pressure ($<10^{-3}$ mbar) at 130°C before use.^[16a]

AlN nanoparticles: 66 mg of AlCl_3 were dissolved in 10 mL of liquid ammonia at -35°C to obtain a colorless solution. Thereafter, 83 mg of KNH_2 were added, which resulted in the precipitation of a colorless aluminum amide-aluminum imide intermediate. This suspension was stirred for an additional 10 min and then naturally warmed to room temperature. After evaporation of all NH_3 , a colorless fluffy solid remained. This solid was dispersed in 15 mL of $[\text{BMIm}][\text{NTf}_2]$ as the ionic liquid. Subsequent to intense mixing, the suspension was rapidly heated (120 s) with a laboratory microwave oven (CEM MARS6) to 300°C . This temperature was maintained for an additional 15 min. After natural cooling to room temperature, the obtained orange suspension was diluted with 15 mL of acetonitrile. The as-prepared AlN nanoparticles were finally purified, KCl as a by-product was removed by centrifugation/redispersion in/from methanol or acetonitrile. Methanol was used here due to its higher solubility of KCl. The AlN nanoparticles can be easily redispersed in acetonitrile or dried at room temperature in a vacuum to obtain AlN powder samples.

Analytical Tools

TEM and HAADF-STEM were performed with a FEI Osiris ChemiSTEM microscope (FEI, The Netherlands) at 200 keV electron energy. TEM samples were prepared by evaporating small droplets of a nanoparticle suspension in acetonitrile onto an ultrathin amorphous carbon film (3 nm) on holey carbon support film mounted on Cu mesh grids (Ted Pella Inc., USA). The loaded grids were subsequently dried under reduced pressure ($<10^{-3}$ mbar) at 120°C for 16 h to remove residual acetonitrile. At least 600 nanoparticles on different TEM images, acquired using TEM Imaging and Analysis (version x, FEI, The Netherlands), were statistically evaluated to determine the mean particle diameter. HRTEM images were further evaluated by calculating the 2D-FT, which yielded information on the crystal structure (lattice parameters and crystal symmetry) of single nanoparticles. The analysis was performed by comparing the experimental 2D-FT and the calculated diffraction patterns with Miller indices, where the latter were obtained by using the JEMS software (Java version of the electron microscopy simulation).^[27]

EDXS was applied to obtain the element distributions within the samples. To address this concern, EDXS elemental maps were recorded by using a Super-X EDXS system comprising four silicon drift detectors (Bruker, Germany), which is installed at the FEI Osiris microscope. The chemical composition of nanoparticles was determined by the quantification of EDXS maps performed using the ESPRIT software (version 2.3, Bruker). Using ESPRIT, element concentrations were calculated on the basis of a refined Kramers' law model, which includes corrections for detector absorption and background subtraction. For this purpose, standard-less quantification, i.e., by means of theoretical sensitivity factors, without thickness correction was applied.

FT-IR spectra were recorded with a Bruker Vertex 70 FT-IR spectrometer (Bruker, Germany). Spectra were obtained using attenuated total reflection (ATR) with the metal-nitride powders in a special optical cell under argon.

XRD was conducted on a Stadi-P diffractometer (Stoe, Germany) with Ge-monochromatized $\text{Cu-K}\alpha_1$ radiation ($\lambda = 1.540598 \text{ \AA}$). Powder

samples were measured in glass capillaries (\varnothing : 0.3 mm), which were sealed under argon.

UV-vis spectra of powder samples were recorded on a Shimadzu UV-2700 spectrometer, equipped with an integrating sphere, in a wavelength interval of 220–800 nm against BaSO_4 as reference. 5 mg of nanoparticles were pestled with dried BaSO_4 and filled into an air-tight sample holder inside an Ar-filled glovebox. Afterwards, the Ar-filled sample holder was transferred to the spectrometer for measurement.

PL Excitation and emission spectra were recorded using a PL spectrometer, Horiba Jobin Yvon Spex Fluorolog 3, equipped with a 450 W Xenon lamp, double monochromators for excitation and emission, an integrating sphere (Ulbricht sphere), and a photomultiplier as detector.

The determination of the quantum yield was performed according to Friend et al.^[28] First of all, the diffuse reflection of the samples was determined under excitation conditions. Thereafter, the emission was measured at this excitation wavelength. Integration over the reflected and emitted photons by use of the Ulbricht sphere resulted in the absolute quantum yield. Corrections were made regarding the spectral power of the excitation source, the reflection behavior of the Ulbricht sphere, and the sensitivity of the detector. The samples were placed in Ar-filled air-tight cuvettes inside a glove box, transferred to the spectrometer and then measured.

Acknowledgements

The authors acknowledge the Deutsche Forschungsgemeinschaft (DFG) for funding within the project "Liquid-phase synthesis of crystalline metal-nitride nanoparticles with semiconducting properties (NanoNitrid: FE911/10-1, GE 841/28-1)".

Open Access funding enabled and organized by Projekt DEAL.

Conflict of Interest

The authors declare no conflict of interest.

Data Availability Statement

The data that support the findings of this study are available from the corresponding author upon reasonable request.

Keywords: aluminum nitride • liquid-phase synthesis • semiconductor nanoparticles

- [1] S. Nakamura, *Angew. Chem. Int. Ed.* **2015**, *54*, 7770.
- [2] N. Zheludev, *Nat. Photonics* **2007**, *1*, 189.
- [3] a) B. Mazumder, A. L. Hector, *J. Mater. Chem.* **2009**, *19*, 4673; b) U. Banin, *Nanoparticles* (Ed. G. Schmid), Wiley-VCH, Weinheim **2004**, 79.
- [4] a) S. M. Sadaf, S. Zhao, Y. Wu, Y.-H. Ra, X. Liu, S. Vanka, Z. Mi, *Nano Lett.* **2017**, *17*, 1212; b) M.-K. Kwon, J.-Y. Kim, B.-H. Kim, I.-K. Park, C.-Y. Cho, C. C. Byeon, S.-J. Park, *Adv. Mater.* **2008**, *20*, 1253.
- [5] a) Z. Li, R. Li, H. Jing, J. Xiao, H. Xie, F. Hong, N. Ta, X. Zhang, J. Zhu, C. Li, *Nature Catal.* **2023**, *6*, 80; b) C. Kim, G. Hwang, J.-W. Jung, S.-H. Cho, J. Y. Cheong, S. Shin, S. Park, I.-D. Kim, *Adv. Funct. Mater.* **2017**, *27*, 1605975; c) S. M. Kim, S. J. Lee, S. H. Kim, S. Kwon, K. J. Yee, H. Song, G. A. Somorjai, J. Y. Park, *Nano Lett.* **2013**, *13*, 1352; d) J. Sato, N. Saito, Y. Yamada, K. Maeda, T. Takata, J. N. Kondo, M. Hara, H. Kobayashi, K. Domen, Y. Inoue, *J. Am. Chem. Soc.* **2005**, *127*, 4150.

- [6] a) G. Tagliabue, J. S. DuChene, M. Abdellah, A. Habib, D. J. Gosztola, Y. Hattori, W.-H. Cheng, K. Zheng, S. E. Canton, R. Sundaraman, J. Sá, H. A. Atwater, *Nature Mater.* **2020**, *19*, 1312; b) H. Lim, J. L. Young, J. F. Geisz, D. J. Friedman, T. G. Deutsch, J. Yoon, *Nature Commun.* **2019**, *10*, 3388; c) J. Winnerl, M. Kraut, S. Artmeier, M. Stutzmann, *Nanoscale* **2019**, *11*, 4578.
- [7] a) R. E. Karaballi, Y. E. Monfared, M. Dasog, *Chem. Europ. J.* **2020**, *26*, 8499; b) C. Giordano, M. Antonietti, *Nano Today* **2011**, *6*, 366.
- [8] L. Xu, S. Li, Y. Zhang, Y. Zhai, *Nanoscale* **2012**, *4*, 4900.
- [9] X. Fang, Y. Bando, U. K. Gautam, C. Ye, D. Golberg, *J. Mater. Chem.* **2008**, *18*, 509.
- [10] a) T. S. Hua, B. Zhu, R. G. Song, *Surf. Eng.* **2020**, *36*, 55; b) R. Vogel, A. K. Pal, S. Jambhrunkar, P. Patel, S. S. Thakur, E. Reátegui, H. S. Parekh, P. Saá, A. Stassinopoulos, M. F. Broom, *Sci. Rep.* **2017**, *7*, 17479; c) M. I. Lerner, E. A. Glazkova, A. S. Lozhkomoiev, N. V. Svarovskaya, O. V. Bakina, A. V. Pervikov, S. G. Psakhie, *Powder Technol.* **2016**, *295*, 307; c) F. Qian, M. Brewster, S. K. Lim, Y. Ling, C. Greene, O. Laboutin, J. W. Johnson, S. Gradecak, Y. Cao, Y. Li, *Nano Lett.* **2012**, *12*, 3344; d) M. Iwata, K. Adachi, S. Furukawa, T. Amakawa, *J. Phys. D* **2004**, *37*, 1041.
- [11] a) M. I. Lerner, E. A. Glazkova, A. S. Lozhkomoiev, N. V. Svarovskaya, O. V. Bakina, A. V. Pervikov, S. G. Psakhie, *Powder Technol.* **2016**, *295*, 307; b) Y. Ma, K. Huo, Q. Wu, Y. Lu, Y. Hu, Z. Hu, Y. Chen, *J. Mater. Chem.* **2006**, *16*, 2834; c) Q. Wu, Z. Hu, X. Wang, Y. Chen, Y. Lu, *J. Phys. Chem. B* **2003**, *107*, 9726; d) J. A. Haber, P. C. Gibbons, W. E. Buhro, *Chem. Mater.* **1998**, *10*, 4062; e) P. D. Ramesh, K. J. Rao, *Adv. Mater.* **1995**, *7*, 177.
- [12] a) J. Buha, I. Djerdj, M. Antonietti, M. Niederberger, *Chem. Mater.* **2007**, *19*, 3499; b) T. Yamakawa, J. Tatami, T. Wakihara, K. Komeya, T. Meguro, K. J. D. MacKenzie, S. Takagi, M. Yokouchi, *J. Am. Ceram. Soc.* **2006**, *89*, 171; c) Q. Zhang, L. Gao, *J. American Ceramic Soc.* **2006**, *89*, 415. d) K. Kim, *J. Crystal Growth* **2005**, *283*, 540.
- [13] A. Fischer, J. O. Mueller, M. Antonietti, A. Thomas, *ACS Nano* **2008**, *2*, 2489.
- [14] a) A. Paseuth, S. Shimada, *J. Am. Ceram. Soc.* **2008**, *91*, 1129; b) C. N. R. Rao, G. Gundiah, F. L. Deepak, A. Govindaraj, A. K. Cheetham, *J. Mater. Chem.* **2004**, *14*, 440.
- [15] W. Cho, Z. Zhou, R. Lin, J. C. Ondry, D. V. Talapin, *ACS Nano* **2023**, *17*, 1315.
- [16] a) T. Welton, *Chem. Rev.* **1999**, *99*, 2071; b) P. Wasserscheid, W. Keim, *Angew. Chem. Int. Ed.* **2000**, *39*, 3772.
- [17] N. E. Christensen, I. Gorczyca, *Phys. Rev. B* **1993**, *47*, 4307.
- [18] M. Hanbücken, P. Müller, R. B. Wehrspohn, *Mechanical Stress On The Nanoscale*, Wiley-VCH, Weinheim **2011**.
- [19] a) N. M. Hwang, J. H. Hahn, D. Y. Yoon, *J. Cryst. Growth* **1996**, *160*, 87; b) D. S. Zhao, M. Zhao, Q. Jiang, *Diam. Relat. Mater.* **2002**, *11*, 234.
- [20] H. F. Gaiser, R. Popescu, D. Gerthsen, C. Feldmann, *Chem. Commun.* **2020**, *56*, 2312.
- [21] P. R. ten Wolde, D. Frenkel, *Phys. Chem. Chem. Phys.* **1999**, *1*, 2191.
- [22] I. Akasaki, M. Hashimoto, *Solid State Commun.* **1967**, *5*, 851.
- [23] H. Schulz, K. H. Thiemann, *Solid State Commun.* **1977**, *23*, 815.
- [24] a) I. A. Khan, B. Hassan, S. A. Hussain, S. Pervaiz, *J. Optoelectron. Adv. Mater.* **2021**, *23*, 373; b) M. P. Thompson, G. W. Auner, T. S. Zheleva, K. A. Jones, S. J. Simko, J. N. Hilfiker, *J. Appl. Phys.* **2001**, *89*, 3331.
- [25] J. Owen, L. Brus, *J. Am. Chem. Soc.* **2017**, *139*, 10939.
- [26] T. Welton, *Chem. Rev.* **1999**, *99*, 2071.
- [27] <http://www.jems-saas.ch/>.
- [28] J. C. de Mello, H. F. Wittmann, R. H. Friend, *Adv. Mater.* **1997**, *9*, 230.

Manuscript received: April 24, 2025

Revised manuscript received: July 2, 2025

Version of record online: